JCTC Journal of Chemical Theory and Computation

Mechanical Properties of Coarse-Grained Bilayers Formed by Cardiolipin and Zwitterionic Lipids

Martin Dahlberg* and Arnold Maliniak

Division of Physical Chemistry, Arrhenius Laboratory, Stockholm University, S-106 91 Stockholm, Sweden

Received December 4, 2009

Abstract: Lipid shape and charge are connected with the physical properties and the biological function of membranes. Cardiolipin, a double phospholipid with four chains and the potential of changing its charge with pH, is crucially connected with mitochondrial inner membrane shape, and recent experiments suggest that local pH changes allow highly curved local geometries. Here, we use a coarse-grained molecular dynamics model to investigate the mechanical properties of cardiolipin bilayers, systematically varying the headgroup charge and the composition in mixtures with zwitterionic 1,2-dioleoyl-glycero-3-phosphatidylcholine (DOPC) or 1,2-dioleoyl-glycero-3-phosphatidylethanolamine (DOPE). Low cardiolipin charge, corresponding to low pH, was found to induce bending moduli on the order of $k_B T$ and curved microdomains. On the length scale investigated, in contrast to continuum theoretical models, we found the area modulus and bending modulus to be inversely correlated for mixtures of cardiolipin and DOPC/DOPE, explainable by changes in the effective headgroup volume.

Introduction

The physical and mechanical properties of lipid bilayer membranes are central for understanding their shapes and functions.[1–3] The strong connection between biological function and membrane properties is highlighted in the mitochondrion, which plays an important role in energy production in eukaryotic cells and has the ability to drastically change its morphology.[4–7] The understanding of the mitochondrial architecture has been expanded recently due to detailed electron microscopy images, and the highly convoluted inner mitochondrial membrane (IMM) is now believed to be composed of distinct, but dynamic, regions. The emerging picture is that proteins and lipids dynamically optimize the mitochondrial topology to adjust performance.[8] It is known that proteins are involved in the organization of mitochondrial and cristae structure[5,9] and that lipid type and composition affect membrane proteins.[10] Recent experiments on model lipid vesicles with a composition close to that of the IMM show that small amounts of locally applied acid can give deformations of the membrane in the shape of tubes with an approximate radius of 40 nm, highly reminiscent of the native mitochondrial tubules and cristae junctions.[11] A deeper understanding for the lipid components of mitochondria is needed to explain the connection between topology and function, both of which are affected by the lipid composition.[12] We thus focus on the lipid components of the IMM. The major IMM lipid constituents are the zwitterionic phosphatidylcholines (PC) and phosphatidylethanolamines (PE) and the negatively charged cardiolipins (CL).[13] The membrane composition varies with species and cell type, but in eukaryotes, the typical ratios of PC:PE:CL are 2:2:1−6:3:1. In the eukaryotes, CLs are specific to mitochondria and typically show a distinct saturation/length pattern in their four acyl chains.[14] The CL headgroup is negatively charged at physiological pH, but different experiments have shown either a net −1 or −2 charge,[15,16] labeled below as CL-1 and CL-2, respectively. The high second pK_a (7.5−9.5) needed to explain the −1 charge at neutral pH has been attributed to intramolecular hydrogen bonding in the CL headgroup. It has also been hypothesized that the ability to trap and conduct protons is important to the proton transport in mitochondrial adenosine triphosphate (ATP) production. Additionally, low pH has been shown to induce negative curvature in CL aggregates (such as the inverse

* Corresponding author e-mail: martind@physc.su.se.

10.1021/ct900654e
Published on Web 04/08/2010

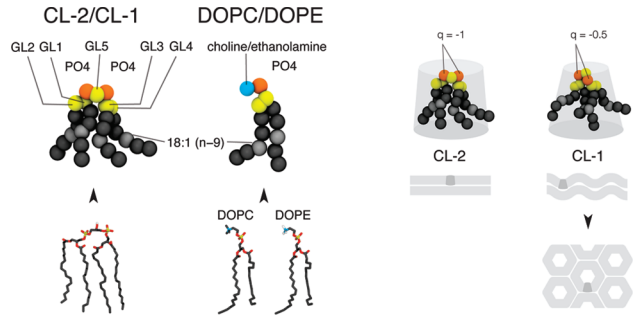

Figure 1. CG models for CL and DOPC/DOPE with 18:1 oleoyl chains. Phosphate charges in CL-2 and CL-1 are −1/−1 and −0.5/−0.5, respectively. The effective geometry of the lipids determines phase behavior. On the right, cylindrical CL-2 (bilayers) and inverse cone-shaped CL-1 (undulating bilayers and the inverse hexagonal phase, H_{II}).

hexagonal phase), and charge neutralization is strongly connected to the propensity to form nonlamellar aggregates with negative curvature.[17] This behavior, and the experimental evidence for tubule formation upon local pH reduction, is not understood mechanistically, and the link between lipid charge and membrane mechanical properties deserves more attention.

Here we present coarse-grained (CG) molecular dynamics simulations of the CL−DOPC and CL−DOPE systems (Figure 1), based on the interaction model proposed by Marrink et al.[18] Our aims are to construct a minimal IMM representation and to examine its mechanical properties. By adding DOPC or DOPE to CL bilayers, we study how the headgroup size and the bilayer charge affect the bending and area modulus of the bilayers. The bending modulus is especially important for understanding the folds of the inner mitochondrial membrane. To further investigate the properties of CL bilayers under stress, we calculate the critical tension for porated bilayers and show how the bilayer line tension is dependent on the composition. We discuss previously reported experiments that suggest the critical tension (or lysis tension) is lowered by introducing small amounts of CL.[19] In a recently developed CG model of CL, the headgroup charge was shown to strongly influence the phase behavior of the lipid aggregates and was shown to reproduce the CL phase polymorphism upon changes in the number of acyl chains and the headgroup charge.[20] Reducing the phosphate charge per molecule from −2 to −1 (in that study scaled down to −1.4 and −0.7) led to adoption of the inverse hexagonal phase (H_{II}), in agreement with experimental observations where the lamellar, to inverse hexagonal phase transition, occurred at pH 2.8.[21] The total bilayer charge was varied in two ways: by changing the concentration of the charged lipid and by changing the protonation state of the charged lipid. Because we chose the acyl chains of all lipids to be identical, we avoided the problem of confounding changes in properties originating from different headgroup characteristics and from those due to chain composition. Generally, lipids with small headgroups and/or large chain volume will form aggregates with negative spontaneous curvature, i.e. inverted phases. The CG models of DOPC and DOPE differ in the interaction parameters of one particle in the headgroup. Effectively, this gives two different headgroup volumes, which affects the spontaneous curvature (see Figure 1). With these two lipids, and the charged CL, we can systematically vary the spontaneous curvature and the effective membrane charge. It is unclear at what composition the lamellar to H_{II} phase transition ought to occur in mixtures of reduced charge CL (−1) and DOPC, but it has been observed experimentally that PC lipids stabilize CL in the lamellar phase.[22] The H_{II} phase is not expected in systems composed of DOPC and CL with full (−2) charges because both components alone form lamellar phases. Aggregates formed by DOPE and CL with reduced (−1) charge have negative spontaneous curvatures and under certain conditions show preference for inverted phases, due to relatively small headgroups. We emphasize that the lamellar bilayer is not the equilibrium aggregate geometry for such lipids, but that for our initial conditions, i.e. intact bilayers, the barrier for phase transition is high. It is, however, instructive to examine the properties of membranes under increasing amounts of frustration due to increased (negative) spontaneous curvature of the monolayers, especially because these changes can be triggered locally with pH changes. The connection between curvature and composition is important in bacterial membranes, where it has also been observed that PE and CL are involved in forming microdomains and that these domains are coupled with the membrane curvature.[23] Interestingly, the syntheses of the two lipids are regulated together,[24] and the lipids can replace some of each others' cellular functions.[25,26]

Based on continuum models for membranes,[27,28] the effects of charge on membrane properties have been described in various limits of electrolyte composition and surface geometry.[29–31] Overall, the electrostatic interactions are suggested to increase membrane rigidity. For mixtures with the possibility of segregating, unstable solutions are found, and the rigidity can instead be lowered as segregation occurs. Experimentally, determining the mechanical properties of mixtures of charged and uncharged lipids have been difficult, showing little or no effect of charged lipids,[32] but recently, Rowat et al. described increases in the electrostatic bending rigidity on the order of 3−5 k_BT for ionic surfactants added to DMPC vesicles.[33]

Recent molecular dynamics (MD) modeling of CL bilayers has shown that CL tends to increase membrane order and decrease lipid mobility,[34–36] which is similar to the behavior found in simulations of other charged lipids.[37] The lipid compositions in the previous MD simulations have been at pure CL or near-physiological CL concentrations, and to our knowledge there are no reports on CL membrane properties over a broad composition range. Atomistic MD simulations give highly detailed information about the specific interactions that occur in these lipid mixtures but are relatively expensive for systematic exploration of mechanical properties. CG approaches have shown much progress in recent years and reproduce many of the important mechanical and structural properties of lipid membranes.[38]

Methods

Model. The CG model used in the previous work[20] (Figure 1) was modified to fit the updated MARTINI07[18] force field:

(i) an increased headgroup charge, to −1.0 per phosphate group, in line with the increased ion charge in MARTINI07. Note that the dielectric constant was decreased from 20 to 15; (ii) the particle type of the unsaturated part of the acyl chain was changed from C1 to C3; and (iii) the GL1−GL2 bond distance was reduced from 0.47 to 0.37 nm.

To better fit the CL geometries from atomistic simulations,[34] the headgroup potentials were optimized (details are given in the Supporting Information). For the CL-1 (−1 total charge) system, the phosphate charges were reduced from −1 to −0.5 each, to model proton equilibration between the two phosphate groups, which was assumed to be rapid compared to the simulation time scale based on recent density functional theory (DFT) calculations of the CL headgroup done in our group.[39] These calculations show that proton exchange between the two phosphate groups is possible on the nanosecond time scale. In the CG model, the reduced charge induced an intramolecular P−P distance shift from 0.60 to 0.58 nm. As a test of the charge partition model, we also studied the −1/0 case in a 1:1 mixture of DOPC and CL.

Models for DOPC, DOPE, water, "antifreeze", and sodium counterions from MARTINI07 were used. For the line tension simulations, antifreeze particles were necessary to avoid crystallization of the solvent, and approximately 10% of the water particles were replaced by antifreeze. Electrostatic and Lennard-Jones interactions were cutoff at 1.2 nm, with electrostatics shifted from 0 to the cutoff and Lennard-Jones interactions shifted from 0.9 nm to the cutoff, as described in MARTINI07.[18] Additionally, a 2.0 nm electrostatic cutoff was tested for the DOPC and CL-2 systems.

Computational Details. Simulations were run employing GROMACS 4,[40] with a 20 fs time step. The time scale was multiplied by a factor of four after simulations to match the experimental diffusion coefficient of water. The temperature was kept at 310 K with a Berendsen thermostat with coupling constant 1 ps. Pressure coupling was carried out using Berendsen barostats set to 1 bar and coupling constant 4 ps. A Nosé-Hoover thermostat (1 ps) and Parrinello-Rahman barostats (semi-isotropic at 10 ps) were also used to test the effect of noncanonical sampling in the Berendsen weak-coupling simulations.

Different compressibilities were used to enable calculation of the mechanical properties. For the line tension system, we used semi-isotropic pressure coupling with zero compressibility in the bilayer slab direction and 5×10^{-5} bar^{-1} in the other directions. In the area compression modulus simulations, compressibilities were set to 5×10^{-5} bar^{-1}, and surface tensions 5, 10, and 15 mN/m were applied in the bilayer plane (NPγT). Critical tension simulations were run similarly but with higher surface tensions (ranging from 30 to 60 mN/m). For all other simulations, semi-isotropic barostats with compressibility 5×10^{-5} bar^{-1} was used. For the pressure profile simulations, we used the local pressure calculations with an Irving−Kirkwood contour, as implemented by Lindahl et al.,[41] in GROMACS 3.0.2 with local pressure extensions. Total simulation times were dependent on which physical property was investigated: (i) 8 μs for the area per lipid and bending modulus; (ii) 4.8 μs for line tensions; (iii) 1.2 μs for area moduli with applied surface tensions; (iv) variable between 10 ns and 1.6 μs depending on the point of collapse for the critical tension simulations; and (v) 300 ns for pressure profiles. Simulation times were chosen to allow proper averaging of the mechanical properties studied.

Systems. Bilayers with 376 CL molecules (188 in each leaflet), based on previous work,[20] were used as a starting point. Pairs of DOPC molecules were generated from CL by splitting the position of the GL5 particle, moving the new choline particles along the GL5−PO_4 bond vectors, and from energy minimization. The mole fractions (X_{CL}) of CL generated were 0, 0.10, 0.25, 0.33, 0.50, 0.67, 0.75, and 1. The substitution was symmetric with respect to the bilayer leaflets. Bilayers with DOPE were obtained by changing the identity of the choline particles in DOPC molecules. No other changes were necessary. Water content was approximately 47 water molecules per lipid, counting each water particle as four water molecules and each CL as two lipids. This is approximately 50% higher than the water content needed to saturate zwitterionic bilayers and corresponds to fully hydrated CL bilayers.[42] We additionally simulated the $X_{CL} = 1$ system with approximately 147 waters per lipid to assess the effect of hydration.

Bilayer pores for critical tension simulations were generated by introducing a new interaction site with strong repulsion only affecting the acyl chain particles. The Lennard-Jones parameter C12 from the interaction level "IX" (0.02581 kJ mol^{-1} nm)^{12} was scaled up to give a pore of sufficient radius. A column of 13 such particles with a spacing of 0.7 nm was introduced across the bilayers. The bilayers were then energy minimized in two steps, first by scaling the repulsion parameter with a factor 10 and then with a factor 1000. The positions of the column particles were not updated, which left them stationary throughout the simulations. Line tension simulations were done with slabs of bilayers (376 CL through 752 DOPC) surrounded by water boxes in the y- and z-directions.[43]

Results

Lipid Segregation. CL charge was found to greatly influence the properties of the bilayers. This was expected because of the propensities to adopt different phases at equilibrium, but we found that even small amounts of CL produced significant qualitative differences between the CL-1 and CL-2 systems. For CL-1, we observed partial lipid segregation, which did not emerge for any concentration of CL-2. Qualitatively the domains can be seen in Figure 2B, where the tighter packing of CL-1 headgroups tended to expose more hydrocarbon chains to water. Two quantitative measures of lipid segregation were investigated: the difference number density, $\Delta\rho$, and the phosphate−phosphate radial distribution functions (rdf) in the bilayer plane. We constructed $\Delta\rho$ by binning phosphate particles of the two leaflets separately onto grids and by taking differences in the number densities along the bilayer normal. The mean absolute $\Delta\rho$, see Figure 2C, was significantly higher in the CL-1 systems for all concentrations except 10% CL. Grid

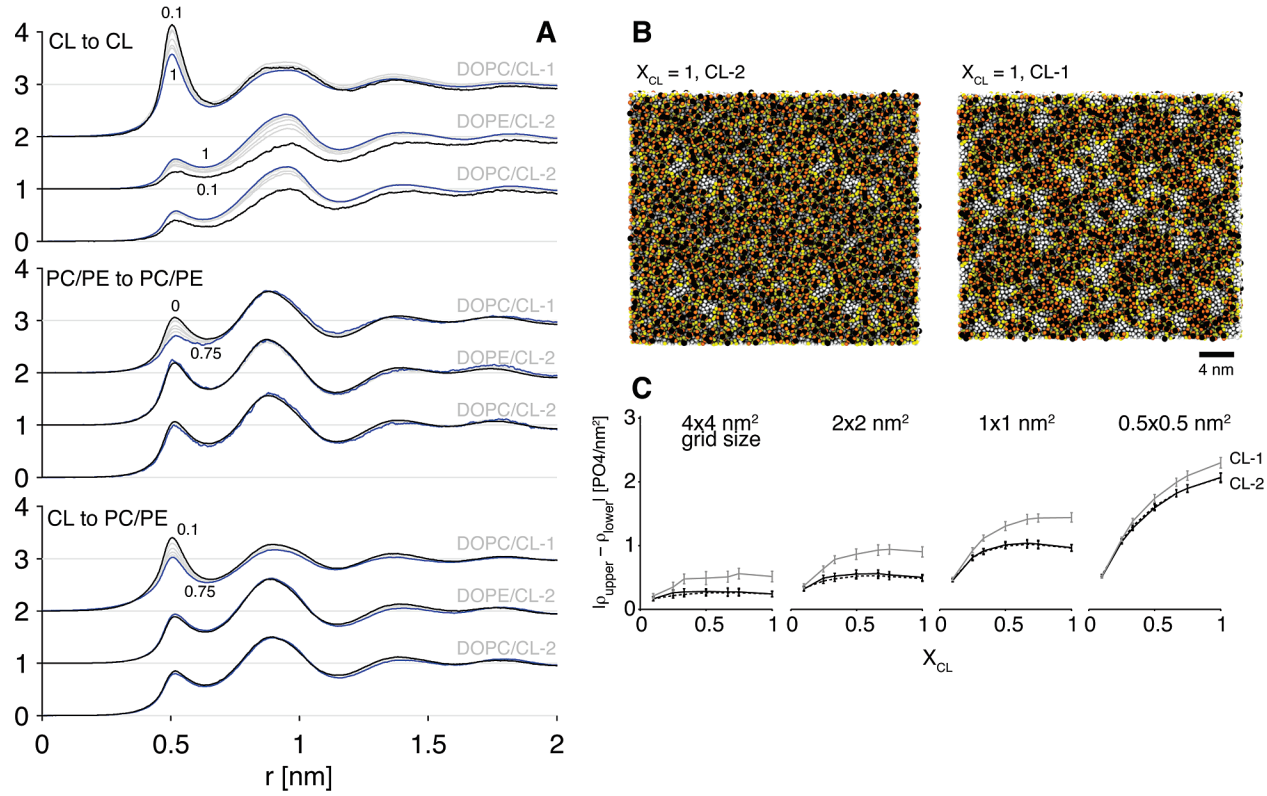

Figure 2. (A) Radial distribution functions two-dimensional (2D) of PO_4 particles for all compositions. Lowest X_{CL} is in black, highest in blue, intermediate in gray, and 10 point moving average; PC/PE represent DOPC or DOPE. (B) Snapshots of microdomain formation in $X_{CL} = 1$, CL-2 left, CL-1 right, and scale bar 4 nm. Hydrocarbon chains in white, and center glycerol (GL5) in black. (C) $\Delta\rho$ for decreasing grid size (4×4, 2×2, 1×1, and 0.5×0.5 nm^2). DOPC/CL-2 (black), DOPE/CL-2 (dotted black), DOPC/CL-1 (gray). Error bars are standard deviations.

sizes between approximately 0.5×0.5 to 4×4 nm^2 were tried, and the largest difference between $\Delta\rho_{CL\text{-}1}$ and $\Delta\rho_{CL\text{-}2}$ was found for grids of size 1×1 to 2×2 nm^2, which gives a semiquantitative view of the size of the domains. Radial distribution functions (Figure 2A) showed that the main effect of lowering CL charge was not primarily to induce segregation of CL-1 and DOPC into separate clusters but rather to bind either lipid more closely to CL-1. Such effects were larger for CL itself, resulting in a dramatic increase in the CL−CL first peak (Figure 2A) and a slightly increased first peak in the DOPC−CL and DOPE−CL systems. The increase in the first peak was compensated by a decrease in the second peak of the CL−DOPC/DOPE rdf.

Association of several CL-1 molecules into dynamic domains induced locally concave surfaces, consistent with negative spontaneous curvature, and was strong enough to expose more of the hydrocarbon chains to the aqueous phase (see Figure 2B). Because the bilayers were constructed with identical composition in the two leaflets, local negative curvature in one leaflet was limited by the hydrocarbon−water surface tension of the corresponding positive curvature in the opposite leaflet. To better understand these changes in the structure of the bilayers, we investigated the main properties that are commonly used to describe mechanical properties in bilayers: the area per lipid, the area compression and bending moduli, the line tension, and the critical tension.

Area Per Lipid. The area per lipid was calculated from the box area divided by the number of two-chained lipid equivalents per leaflet and is shown in Figure 3F. Pure CL had an area of 0.631 ± 0.003 nm^2, which was lower than the area of DOPC (0.682 ± 0.002 nm^2) and slightly lower than DOPE (0.647 ± 0.002 nm^2). It should be noted that, experimentally, the DOPE area per lipid at 310 K is not known, because DOPE is not stable in the lamellar phase at that temperature. At 271 K, where DOPE is in the lamellar phase, the area was 0.65 nm^2,[44] which compares favorably with the simulated value, but previous CG simulations with the first generation of the model used here, but at 273 K, showed a lower area of 0.61 nm^2.[45] The CL area was slightly lower with the updated CL model (0.631 vs 0.643 nm^2), which reflects the updated headgroup bond lengths and angles as well as the changed dielectric constant and the use of full ion charges. The DOPC area was in reasonable agreement with recent experiments (0.669 at 303 K)[46] and comparable to the CG model at 300 K (0.67 nm^2).[45]

The reduced charge model, CL-1, had a lower area per lipid, 0.596 ± 0.005 nm^2, consistent with reduced intra- and intermolecular electrostatic repulsion. It should be noted that the undulations for pure CL-1 were very strong and that undulations tend to reduce the area per lipid defined as the area projected onto the xy plane. The −1/0 charged CL model at $X_{CL} = 0.5$ gave an average area per lipid in close agreement (0.616 ± 0.006 nm^2) with the −0.5/−0.5 model (0.610 ± 0.007 nm^2), showing that the effects are not specific to the choice of charge partition.

For all three investigated systems, the area per lipid dependence of the composition was nonideal (as seen in Figure 3F), with a lower area per lipid than a linear

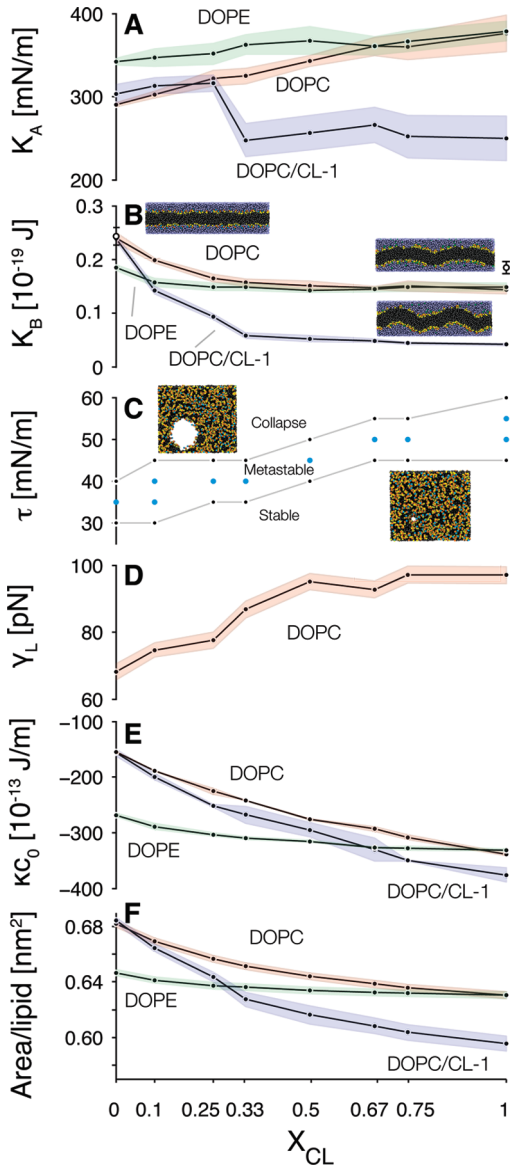

Figure 3. Mechanical properties as a function of mole fraction CL:DOPC and DOPE indicate DOPC/CL-2 and DOPE/CL-2, respectively. From top to bottom: (A) Elastic area compression modulus, K_A. Uncertainties (shaded) are standard deviations from a linear fit to the γ-A isotherms. (B) Bending modulus, K_B. Uncertainties (shaded) are standard deviations from five parts of the 8 μs trajectory. Inset images are snapshots showing bilayer undulations for mole fractions 0 and 1. Open symbols denote an electrostatic cutoff of 2.0 nm. (C) Critical tension, τ. Border between bottom (stable > 1 μs), metastable (40−1000 ns), and collapse (<40 ns) was determined by repeated simulations starting with a porated bilayer. Inset images are snapshots from X_{CL} 0.5 bilayers with a preformed pore at surface tension 40 and 45 mN/m. (D) Line tension, γ_L, for the DOPC/CL-2 bilayer ribbon systems. Uncertainties (shaded) are standard deviations. (E) First moment of lateral pressure profile, κc_0. Uncertainties (shaded) are standard deviations between upper and lower leaflets. (F) Area per lipid (CL counted as two lipids). Uncertainties (shaded) are standard deviations.

combination of the pure components. For a given mole fraction, the deviation from ideality was larger in DOPC/CL-2 than in DOPE/CL-2, which implies that the canonical area per lipid for CL-2 was smaller with DOPC than with DOPE.

Table 1. P−N Vector Tilt Angle in DOPC or DOPE Relative to the Bilayer Normal[a]

	DOPC/CL-2	DOPE/CL-2	DOPC/CL-1
$X_{CL} = 0.75$	74.4 ± 0.1	86.3 ± 0.1	71.62 ± 0.09
$X_{CL} = 0.67$	74.5 ± 0.1	86.1 ± 0.1	71.8 ± 0.1
$X_{CL} = 0.5$	74.52 ± 0.06	85.6 ± 0.1	72.4 ± 0.1
$X_{CL} = 0.33$	74.66 ± 0.05	84.92 ± 0.07	73.0 ± 0.1
$X_{CL} = 0.25$	74.68 ± 0.08	84.41 ± 0.05	73.12 ± 0.07
$X_{CL} = 0.1$	74.48 ± 0.03	83.08 ± 0.04	73.59 ± 0.03
$X_{CL} = 0$	73.83 ± 0.04	81.33 ± 0.04	73.75 ± 0.02

[a] Errors are standard errors of the mean (SEM) from two leaflets, and trajectory is split into five equal length parts.

The area per lipid of tetraoleoyl−CL is not known, but Goormaghtigh et al. estimated that saturated or unsaturated CL has a surface area of 1.2 nm^2,[47,48] which compares favorably to our results (1.26 and 1.19 nm^2 for CL-2 and CL-1, respectively). Previous all-atom simulations of pure CL bilayers gave an area per lipid of 0.99 nm^2,[34] which corresponds approximately to the experimental area of saturated tetramyristoyl−CL, estimated to 0.5 nm^2 (per two chains) in the fluid lamellar phase.[49] Ion binding in the carbonyl region reduced the area per lipid strongly in the MD simulations. In the present CG approach, such ion binding is much less specific and occurs instead at the level of the phosphate groups, resulting in a higher area per lipid. It should also be noted that the areas of the other components are only in semiquantitative agreement with experiments and that the balance of forces which determine the area will be dependent on all components of the mixture.

As a further characterization of the lipid behavior of the mixtures, we calculated the P−N tilt angle away from the bilayer normal for DOPE and DOPC (Table 1). The averaged P−N tilt was larger for DOPE than DOPC for all compositions, which is consistent with the smaller headgroup in DOPE. In contrast to the minor changes in the P−N tilt in DOPC, the DOPE headgroup tilted further away from the bilayer normal with increasing CL content, which is consistent with the "voltameter" model.[50] This behavior shows that the response of the P−N dipole to the charge of the bilayer is dependent on the size or interaction parameters of the choline/ethanolamine groups. Both effects, smaller volume and increased potential for hydrogen bonding to the phosphate groups of CL, enable larger P−N tilts in DOPE than in DOPC. For the DOPC/CL-1 system, there was even a small decrease in the tilt angle with increasing CL-1 content. It should be noted that increased local curvature in the DOPC/CL-1 systems makes the P−N definition, where the simulation box is used as the reference coordinate system, less useful for comparing with DOPC/CL-2 and DOPE/CL-2 cases where the undulations were more suppressed.

Compression Modulus. In Figure 3A, the elastic area compressibility modulus (elasticity), K_A, defined as $K_A = A \cdot d\gamma/dA$, for the mixed bilayer systems is shown. A series of simulations with increasing surface tension was performed, and the resulting response in the bilayer area was recorded. The uncertainties reported here are standard deviations from the linear fit to the area surface tension data. The overall trend shows an increase in K_A with $X_{CL\text{-}2}$, the effect being stronger with DOPC than with DOPE. At high

CL concentrations, changing the zwitterionic colipid had no significant effect on K_A. The opposite trend, i.e., decreasing K_A with $X_{CL\text{-}1}$, was observed in the CL-1 system above $X_{CL\text{-}1} = 0.25$, where K_A dropped significantly. The surface charge density, which is similar although not exactly the same in the DOPC and DOPE systems due to different mean areas, was not directly connected to K_A. We also note that if the net charge density was the main factor determining elasticity, we would expect the elasticity modulus at $X_{CL} = 1$ for CL-1 to correspond to the value at $X_{CL} = 0.5$ for CL-2, which is not the case. Continuum membrane models predict the area modulus to be affected most by the chains.[28] Because no changes were made in the acyl chain part, we would, therefore, expect similar K_A for CL-2 and CL-1. However, the packing parameter of the CL-1 lipids turned out to favor lipid segregation with locally increased curvature. The applied surface tension then not only elastically deforms the bilayer but also restricts undulations. This is related to the apparent area compressibility modulus measured in experiments, where the contribution from thermal undulations has to be disentangled from the elasticity and the system size effect seen in MD simulations of lipid bilayers.

Recently, micropipet and monolayer experiments[19] showed that the apparent area expansion modulus, K_A^{app}, was significantly reduced by introducing CL into SOPC vesicles and egg−PC monolayers, respectively. This runs contrary to the results found here for the CL-2 systems. It is necessary, in principle, to consider not only the concentration of the charged CL but also the change in concentration of different chains. Whereas our simulations were run with constant chain composition, the CL used for the experiments contains significantly more unsaturated chains than SOPC or egg−PC. Unsaturated chains tend not to affect K_A strongly, but can lower K_A^{app} due to a decreased bending modulus.[51,52] The effects of charged lipids on the mechanical properties of bilayers were better separated in a study of POPG/POPA in POPC bilayers,[53] where the area compressibility modulus, up to sensitivity of the experiment, was not changed by the inclusion of as much as 30% anionic lipid. A similar result was found for monolayers of pulmonary surfactant simulated with the same CG force field used here,[54] and no significant difference in the area compression modulus was found with charged lipid content.

Bending Modulus. The bending modulus can be calculated by quantifying the thermal undulations of the bilayer.[55] An alternative method based on pulling bilayer tethers, a process not dependent on thermal excitation of the long wavelength undulations, has been proposed recently.[56] Our main goal was to see the systematic changes in the bending modulus and thus opted for avoiding the added complexity of reliably equilibrating the inner and outer leaflets necessary in the tether method.

Spectral densities were calculated by interpolating the positions of all C2 chain particles to an upper and lower leaflet 200 × 200 grid (approximate grid spacing 0.08 nm) and by averaging over the z-position of the grids. Different grid spacings were tried with consistent results. The 2D-Fourier transformed grids for each trajectory frame were integrated in circles from the zero frequency and then averaged over the 8 μs trajectory. The bending modulus was calculated by fitting a q^{-4} function to the longest undulation modes (the three smallest $\mathbf{q}$ vectors were used) on a log−log scale and by setting the additive constant equal to log (k_BT/AK_B) and evaluating for K_B. Uncertainties in the bending moduli were estimated by splitting the trajectory into five equal length parts.

In Figure 3B, the bending modulus from bilayers at zero surface tension is shown. There was a general tendency toward decreasing K_B with the mole fraction of CL. Bilayers with DOPE had a slightly lower K_B than bilayers with DOPC, although above $X_{CL} = 0.33$ the difference was not significant, and K_B was essentially constant. Overall, the bending moduli for the pure zwitterionic bilayers were lower than the experimental value for DOPC (0.85×10^{-19} J)[52] but close to the range found previously in simulations with similar force fields.[45] We expect our bending moduli to be slightly lower than those found for DPPC, due to the unsaturated chains. This is in agreement with a decrease in the bending modulus with decreased saturation and charge for DPPC/POPG mixtures found by Baoukina et al.[54] Experimental DOPE bending moduli calculated from the H_{II} phase were 20% higher than for DOPC.[57]

A radical decrease in K_B was observed when CL-1 was added. Long undulation modes were increasingly excited, and the undulation spectrum also showed concentration dependence in the short-wavelength region (data not shown), absent in CL-2 simulations. Whereas DOPC and DOPE bilayers with CL-2 had bending moduli in the 3−6 k_BT range, CL-1 showed K_B close to 1 k_BT for all $X_{CL} > 0.25$, which is consistent with the strong thermal excitations of long undulation modes. This effect was also seen in the $X_{CL} = 0.5$ simulation (4 μs) with the −1/0 charge partition in the headgroup. Additionally, 4 μs runs of $X_{CL} = 0$ and 1 with the Nosé-Hoover/Parrinello-Rahman combination did not show significant differences in the bending moduli relative to the Berendsen method.

In recent experiments on DMPC vesicles with adsorbed surfactants, charged or uncharged, the charged surfaces exhibited higher bending rigidity.[33] The surface charge density was kept low in those experiments, with less than 5 mol % adsorbed surfactant. As a test of the dependency on electrostatic interactions, we also calculated the bending moduli for the pure CL and DOPC phases with an increased cutoff length on Coulomb interactions (open circles in Figure 3B). Increasing the cutoff from 1.2 to 2.0 nm increased the bending modulus by 27% for CL and 2% for DOPC, and it has been established previously that the surface concentration of counterions tends to increase with an increased cutoff.[20] Because long-ranged electrostatic interactions between adjacent bilayers can suppress undulations, we tested the effect of the amount of water on the bending modulus and found that K_B was lowered slightly: $0.13 \pm 0.01 \times 10^{-19}$ at 147 waters/lipid, and $0.15 \pm 0.01 \times 10^{-19}$ J at 47 waters/lipid. This corresponds to 55% (147 w/l) and 60% (47 w/l) of the bending modulus of DOPC and shows that the effect of including more water is very limited. The increase in ion binding caused by increasing the electrostatic cutoff radius

is most likely part of the reason for the increased cohesive pressure (see Pressure Profiles below).

Critical Tension. As a measure of the stability of the CL bilayers, we subjected bilayers with preformed pores to surface tensions of increasing magnitude. The critical tension was defined as the tension where pore growth was dramatically increased. The time to bilayer collapse was defined, for simulations where collapse was observed, as the simulation time between the onset of applied surface tension and an increase of the projected pore area with a factor of two or more. This definition is arbitrary but gives a simple criterion for dramatic changes to the structure of the bilayer. The critical tension is, in general, dependent on the loading rate.[58] Repeated simulations with our protocol gave critical tensions that were reproducible to within 5 mN/m, which was enough to show the trend of increasing critical tension with CL concentration. When the target surface tension was above the threshold for pore expansion, the actual applied surface tension dropped slightly below the target value. This is expected because the system is not in mechanical equilibrium during pore expansion. In the simulations where a critical tension was applied, the actual surface tension was typically between 93 and 98% of the target tension. Because a large part of pore expansion is doing work against the line tension of the pore, we also measured the line tension with the protocol of Tolpekina et al.[43] The line tension was defined as $\gamma_L = A_{xy}[(P_{yy} + P_{xx})/2 - P_{zz}]/2$, where the bilayer slab is periodic in the z-direction, A_{xy} is the cross section area of the box in the $x-y$ plane, and P_{xx}, P_{yy}, and P_{zz} are the diagonal elements of the pressure tensor.

The increase in line tension with CL concentration is shown in Figure 3C, and the effect was largest for small amounts of CL and turning essentially constant above $X_{CL} = 0.5$. From a geometric point of view, lipids with a positive curvature, e.g., micellar surfactants, can stabilize the edge[59] and thereby allow pore growth. Conversely, inclusion of inverted cone shaped lipids, such as cholesterol, has been shown to increase line tension in DOPC vesicles.[60] Additionally, membranes with PE lipids and anionic PS lipids have been shown to have a higher line tension than neutral PC membranes.[61] By changing the spontaneous curvature through the addition of CL, we thus expected pores to be less likely to expand, which is what we observed in the critical tension simulations. The calculated line tension for DOPC, 68 ± 2 pN, is comparable to previous results with the MARTINI force field (62−64 pN for DPPC/POPG mixtures) but larger than the experimentally determined line tension, which is in the 7−25 pN range.[58,60,61]

Nichols-Smith et al.[19] measured the lysis tension (critical tension) in SOPC membranes with CL. For CL concentrations of 5 and 9.2%, the lysis tension was lowered by 3.5 and 5.1 mN/m, respectively, which is the opposite of what we observe. A possible explanation for the discrepancy is that unsaturated chains (CL was more unsaturated than SOPC) lower the bending modulus and the lysis tension.[51,52] The breakdown voltage for black lipid membranes with the charged lipid phosphatidylserine or PC was about equal and independent of ionic strength.[62] In the same experiments, the chain volume was found to correlate negatively with membrane rupture. Keeping chain volume fixed, as in our model, and instead varying the headgroup volumes, the trend we observed suggests that the correlation carries over from absolute into relative chain volumes, i.e., lower headgroup volumes giving higher lysis tensions.

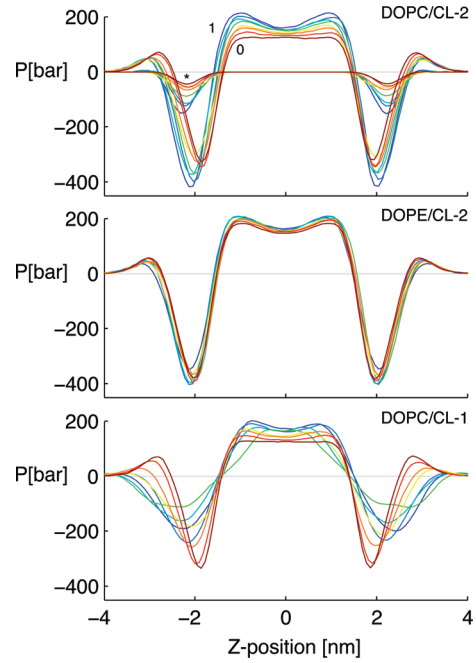

Figure 4. Pressure profiles as a function of distance from center of bilayers, from top to bottom: DOPC/CL-2 with the electrostatic component (*), DOPE/CL-2, and DOPC/CL-1. Colors denote X_{CL} from 0 (red) through 1 (blue).

Pores have two different curvatures: one negative in the bilayer plane and one positive, which has a radius determined by the monolayer thickness, tracing lines orthogonal to the first curvature. Recent simulations show that effects of the negative curvature can be neglected even for radii corresponding to pore closure.[63] Using the relationship between line tension, γ_L, and surface tension, Γ, we calculate an approximate radius at which the calculated line tension for the pore edge balances the surface tension created by opening the pore, i.e., $r = \gamma_L/\Gamma$. The calculated critical pore size by this method was 1.8 ± 0.1 nm across the range of concentrations at the surface tension corresponding to the critical tension and 2.3 ± 0.2 nm at the border between stable and metastable pores. These radii are larger than what was observed in the simulations, where the hydrocarbon pore was ∼1.3 nm, and the water cylinder in the pore was ∼1.1 nm but in qualitative agreement.

Local Pressure Profiles. We investigated the connection between bilayer behavior and interactions in the bilayer by calculating local pressure profiles along the bilayer normal. The pressure profiles for all compositions, shown in Figure 4, were calculated according to Lindahl et al.,[41] and the difference between the lateral and normal pressures was binned into 100 bins (approximately 0.1 nm per bin) along the z-axis. In the DOPC/CL-2 system, there were systematic changes to all three main regions of the pressure profile: the

repulsive chain region, the attractive interface region, and the repulsive headgroup region. The pressure in the chain region increased with CL concentration. In the interface region, there was a shift of about 0.2 nm away from the center of the bilayer in going from $X_{CL} = 0$ to $X_{CL} = 1$. The interface pressure was also increasingly negative. Finally, the outer region had a similar outward shift as the interface peak, but the pressure decreased in magnitude. These changes can be explained by a decrease in the effective headgroup volume, which decreases the headgroup pressure and packs the lipids tighter. The effect can be correlated to the area per lipid, which decreased with the CL mole fraction (see Figure 3E). In the DOPE/CL-2 system, the local pressure profile was practically unchanged with concentration, but had high chain pressures and increased interface attraction as well as lower headgroup repulsion relative to the DOPC/CL-2 system. More drastic changes were observed in the DOPC/CL-1 pressure profiles. The most significant effects were: a reduced interface pressure, a stronger X_{CL} dependence, and a flattening of the headgroup repulsion profile. Reduced headgroup pressure, brought about by decreasing the phosphate charges, is consistent with the partial segregation seen in these systems. A general broadening of the interface was seen, which is explained in part by the increase in undulations. The slight asymmetry seen for the in pressure profile is also due to undulations, which make the interface less well-defined and the pressure statistics poorer.

From a decomposition of the lateral pressures into the respective interactions in the DOPC/CL-2 system, it was found that the electrostatic interactions had a net negative pressure, corresponding to a positive surface tension (see Figure 4). The dominant component of the electrostatic interactions was the CL−ion interaction which generated pressures on the order of −400 bar with $X_{CL} = 0$.

Spontaneous Curvature. As a measure of the tendency to form inverted phases, we used the first moment of the lateral pressure profile, which is proportional to the spontaneous curvature of the monolayer, c_0, and to the bending modulus (here denoted κ): $\kappa c_0 = \int_0^\infty z\Sigma(z)dz$ and is independent of the position of the reference point along the bilayer normal, if the total surface tension is zero and if $\Sigma(z) = \langle P_z(z) - P_{||}(z)\rangle$, where $P_{||}(z)$ is the pressure in the bilayer plane. Negative spontaneous curvature was observed for all systems over the entire CL concentration range (see Figure 3E). The effects of a smaller zwitterionic headgroup (DOPE as compared to DOPC) and of a less charged headgroup (CL-1 as compared to CL-2) were all visible in the spontaneous curvature. Interestingly, the combination of DOPE and CL-2 had a more negative spontaneous curvature for low CL concentrations than that of the CL-1 system with reduced charge.

Order Parameters. The sequential particle−particle order parameters give a molecule centric view of the effects of local environment. Overall, order parameters were very similar for CL and DOPC/DOPE, with differences located mainly in the headgroups, see Figure 5. In the chain region the order was increased slightly with increasing CL-2 concentrations, and the change was the largest near the end of the tails. Headgroup order changes as a function of X_{CL}

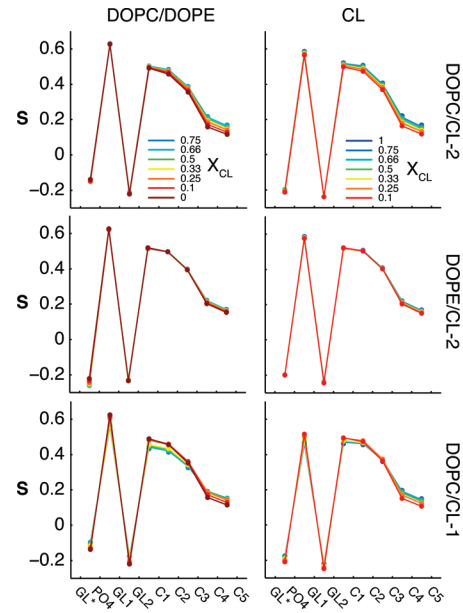

Figure 5. Sequential order parameters, *S*, as a function of position in DOPC/DOPE (left) and CL (right). $X_{CL} = 0$ (red) through $X_{CL} = 1$ (blue).

were minor for both components in the DOPC/CL-2 system. Chain order was slightly higher for DOPE/CL-2 than for DOPC/CL-2, but variations with composition were minute. This is consistent with the pressure profile differences between the systems, where higher chain pressures for DOPE were observed. In the reduced charge systems, the order parameter showed a tendency to decrease for all segments in the polar part of the lipid but tended to increase in the two last segments. The increased chain order can be explained by the lower area per lipid caused by a reduced repulsive interaction between lipids. Undulations and locally increased curvature, both of which were seen with CL-1, tend to weaken order in the polar part of the lipid.

As mentioned above, the effect of increasing the water content perturbs the system only slightly. The order parameters thus were at most decreased by 4% in the 147 w/l system, relative to the 47 w/l system.

Counterion Profiles. A potential shortcoming of these CG models is the treatment of electrostatics. As a guide in judging the effect of neglecting the long-ranged interactions, we calculated the counterion profile in the bilayer normal direction (see Figure 6). Predictably, the ion profiles were essentially flat outside a cutoff distance from the charge headgroups, but the majority of the counterions were adsorbed to the interface, which is the behavior observed in atomistic simulations.[34–36] For mixed DOPC/CL-2 bilayers, the profile showed a minimum just outside the headgroup region, which we attribute to the effect of charge interactions with the P−N dipole and to the shifted balance in the interactions between water and ion particles with the choline particle type. In DOPE bilayers, the dipole tilt is significantly higher, essentially in the bilayer plane, and the ethanolamine particle type is more similar in its interactions with water and ions.

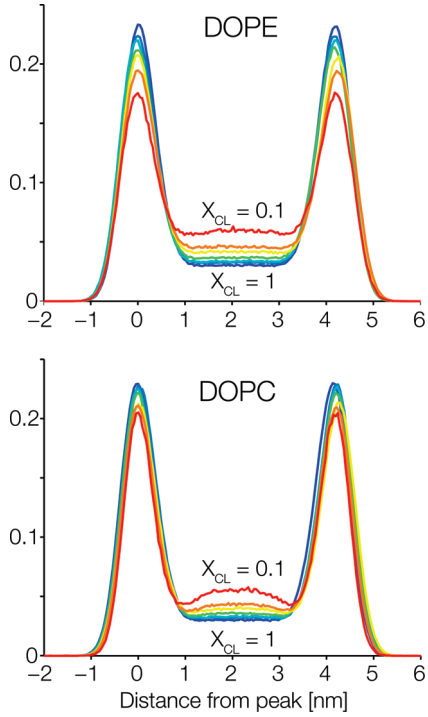

Figure 6. Counterion density distributions for DOPE/CL-2 and DOPC/CL-2 as a function of position along the bilayer normal, with the origin set at the maximum of the distribution. Normalized with the total number of ions in the system. Arbitrary units on the vertical axis. $X_{CL} = 0.1$ (red) through $X_{CL} = 1$ (blue).

Interestingly, the local minimum seen in the PC simulations has also been observed in atomistic simulations.[64,65]

Discussion

The main finding from this coarse grained (CG) model of cardiolipin (CL) membranes was that the rigidity of the bilayer was correlated to the effective headgroup volume, so that small headgroups were associated with lower bending moduli. In contrast to continuum models, where bending deformation of the membrane is directly proportional to the elasticity of the monolayers, the CL with full headgroup charge in our study exhibited an inverse relation between these two quantities. We note that the changes in area and bending moduli for the DOPC and DOPE systems were small and that these differences may not be large enough to be distinguishable experimentally over the range of CL concentrations. The spontaneous curvature aggregate κc_0, calculated from the pressure profiles, was increasingly negative with CL concentrations and lower for DOPE than for DOPC. This is consistent with the notion that small headgroup volumes tend to give negative curvatures, and here we have shown that this was true over the entire concentration range, with κc_0 monotonically decreasing as a function of X_{CL}. In the case of DOPC, the CL headgroup charge was clearly connected to the spontaneous curvature, and we observed microdomain formation when the charge was reduced on each CL. The area elasticity modulus in the CL-1 system was also low, which can be explained as an effect of the decreased bending modulus, which leads to a undulation dominated area dilation with logarithmic increase in area for a given surface tension.[66] The bending modulus in CL-1 was on the order of k_BT, which is consistent with the large undulations seen, and also indicates that the lamellar phase becomes destabilized upon charge neutralization. This effect was not sensitive to the choice of charge partition (−1/0 or −0.5/−0.5) in the headgroup. For DOPE, the X_{CL} dependence of κc_0 was lower, which is explained by headgroup sizes in DOPE and CL-2 being quite similar.

Net attractive interactions (negative lateral pressures) were found for the electrostatics in the headgroup region, increasing with the mole fraction of CL. The dominant component of the electrostatic interactions was between counterions and CL. Smaller in magnitude, and opposite in sign, was the CL−CL component of the pressure. With increasing CL concentration, the combination of increased chain pressure, decreased headgroup repulsion, and a net attractive electrostatic component gave a monotonously decreasing κc_0. It should be pointed out that κc_0 is independent of the position of the pivot plane for pressure profiles with zero surface tension but that the contribution from the components is not. For pivot plane positions close to the interface, the electrostatic component was still found to give a negative contribution to κc_0, i.e. negative curvatures. Thus, introducing headgroups of the same charge is not necessarily associated with reduced interface cohesion, and effective headgroup volume must be taken into account to accurately predict the change in mechanical properties induced by charged lipids.

We found that the line tension increased significantly with CL concentration. We understand this also as a consequence of the average effective headgroup volume, which will force inverse cone-shaped lipids away from pores, thus stabilizing the bilayer. Our two methods, the stability of a porated bilayer under tension and the bilayer ribbon can be seen as opposite extremes of pore radius (∼1 nm and infinite, respectively). Because both methods gave the same trend in the line tension, we conclude that a small pore radius is not stabilized due to the negative curvature of the monolayers. This is in agreement with the results of Wohlert et al.[63] The increase in line tension with CL concentration, also at physiological levels of CL, stabilizes the membrane against pore expansion and rupture, at least on the time and length scales of the present simulations.

A notable feature of the CL−DOPC mixtures was the systematic change in chain pressure just beneath the interface that we observed as a function of the composition. With pressure differences on the order of 100 bar, CL can affect other lipids and membrane proteins even if direct binding of the charged headgroup is not possible. The observed trends can be understood in the context of effective headgroup volume: DOPE and CL with smaller headgroups having an overall larger chain pressure than DOPC. Similarly, small headgroups were associated with high area modulus (high chain pressures), as long as CL charge was high.

The lateral pressure profile is generally built up from large, and to a high degree canceling, components. The balance of forces across the membrane is sensitively dependent on the respective interactions, and the coarse nature of the model presented here does not allow us to predict the behavior of

specific compositions or of spatial detail smaller than approximately 0.5 nm. In our view, we should instead use the systematic variations of easily controlled parameters to get a feeling for the minimum required parameters to model CL membranes. The CG model, which this work is based on, has been shown to reproduce many of the crucial properties of zwitterionic membranes, and our CL model only changes the headgroup interactions and the connectivity. A limiting factor in improving the present model is the lack of experimental results, such as area per lipid, bending modulus, and critical tension, controlled for CL chain composition. The headgroup properties of CL are still not well understood, and further experiments will be needed to determine reliably the CL area and the charge in mixtures with zwitterionic lipids.

The simulations presented in this study, with the exception of the pore simulations, were stable on the microsecond time scale. For DOPC and pure CL-2, we infer from previous modeling work that the equilibrium state is the bilayer. We have observed hexagonal phase formation for DOPE and CL-1 at 310 K, starting from isotropic lipid−water mixtures (DOPE) and stalked bilayer stacks (CL-1) (data not shown). A limitation to the present work is that the true equilibrium properties of the lipid mixtures are not fully known. We thus emphasize that the mechanical properties and the structural features found here only indicate the trends and that they should be interpreted as perturbations of the equilibrium states of the pure and stable bilayer membranes. As such, the local lipid segregation we found with CL-1 mixtures should not primarily be seen as evidence of domain formation in the sense reported recently[67–69] but rather as a mechanism of dissipating curvature frustration when the barrier to phase transition is high due to the high water content. Changing CL charge from −2 to −1 reduces electrostatic repulsion and increases "hydrogen bonding" (determined by the Lennard-Jones parameters), which together lowers the effective size of the headgroup. Because the total curvature in the domains remains fairly small and only small changes in bilayer thickness occurred, it is unlikely that domain formation is driven by a change in the electrostatic screening length, as seen in micelle fission by Sammalkorpi et al.[70]

The transition in bending modulus seen for CL-1 is compatible with the nonequilibrium vesicle system of Khalifat et al.,[11] showing that local pH manipulations (from global pH 8 to estimated local pH 4−5) can cause structural changes in the membrane. We note that the inclusion of CL in either its −1 or −2 state decreased the rigidity of the bilayer, which is compatible with highly curved mitochondrial membranes. Considering a second pK_a in the 7.5−9.5 region for CL, a possible mapping between the charge states in the simulations and the experiments is −2 at pH 8 and −1 at pH 4.

An important limitation of this work is the treatment of the electrostatics. We have quantified this in the counterion profiles, which agree qualitatively with atomistic simulations. However, in the aqueous phase the profiles deviate predictably—due to the cutoff—from the smoothly decaying behavior predicted from a Poisson−Boltzmann treatment. More rigorous coarse graining of electrostatics is being developed by others,[71,72] showing promising results and could be used to improve the model presented here. Another direction is to rationalize the cutoff as an effect of screening by a low amount of (virtual) salt. For Debye lengths comparable to a 1.2 nm cutoff, the monovalent salt solutions are in the 10−60 mM range (with limits taken for effective dielectric constants 15 and 80, respectively), which is low compared to the physiologically relevant salt concentration (approximately 200 mM). Ultimately, using a uniform effective dielectric constant might prove too coarse for charged species at the interface, but the work presented here gives some predictions that can be tested experimentally and with other molecular electrostatic models.

Acknowledgment. We thank Erik Lindahl for fruitful discussions. This work was supported by grants from the Swedish Research Council (VR) and the Carl Trygger Foundation.

Supporting Information Available: Details of the updated coarse grained cardiolipin model. This material is available free of charge via the Internet at http://pubs.acs.org.

Abbreviations. CL, cardiolipin; DOPC, 1,2-dioleoyl-glycero-3-phosphatidylcholine; DOPE, 1,2-dioleoyl-glycero-3-phosphatidylethanolamine; POPC, 1-palmitoyl-2-oleoyl-glycero-3-phosphatidylcholine; POPG, 1-palmitoyl-2-oleoyl-glycero-3-phosphatidylglycerol; POPA, 1-palmitoyl-2-oleoyl-glycero-3-phosphatidic acid; SOPC, 1-stearoyl-2-oleoyl-glycero-3-phosphatidylcholine; DMPC, 1,2-dimyristoyl-glycero-3-phosphatidylcholine; DPPC, 1,2-dipalmitoyl-glycero-3-phosphatidylcholine.

References

(1) Bloom, M.; Evans, E.; Mouritsen, O. G. Physical Properties of the Fluid Lipid-Bilayer Component of Cell Membranes: A Perspective. *Q. Rev. Biophys.* **1991**, *24*, 293–397.

(2) Zimmerberg, J.; Gawrisch, K. The Physical Chemistry of Biological Membranes. *Nat. Chem. Biol.* **2006**, *2*, 564–567.

(3) Marsh, D. Protein Modulation of Lipids, and Vice-Versa, in Membranes. *Biochim. Biophys. Acta* **2008**, *1778*, 1545–1575.

(4) Frey, T. G.; Mannella, C. A. The Internal Structure of Mitochondria. *Trends Biochem. Sci.* **2000**, *25*, 319–324.

(5) John, G. B.; Shang, Y.; Li, L.; Renken, C.; Mannella, C. A.; Selker, J. M.; Rangell, L.; Bennett, M. J.; Zha, J. The Mitochondrial Inner Membrane Protein Mitofilin Controls Cristae Morphology. *Mol. Biol. Cell* **2005**, *16*, 1543–1554.

(6) Mannella, C. A. The Relevance of Mitochondrial Membrane Topology to Mitochondrial Function. *Biochim. Biophys. Acta* **2006**, *1762*, 140–147.

(7) Mannella, C. A. Structure and Dynamics of the Mitochondrial Inner Membrane Cristae. *Biochim. Biophys. Acta* **2006**, *1763*, 542–548.

(8) Benard, G.; Rossignol, R. Ultrastructure of the Mitochondrion and its Bearing on Function and Bioenergetics. *Antioxid. Redox Signaling* **2008**, *10*, 1313–1342.

(9) Heath-Engel, H. M.; Shore, G. C. Mitochondrial Membrane Dynamics, Cristae Remodelling and Apoptosis. *Biochim. Biophys. Acta* **2006**, *1763*, 549–560.

(10) Phillips, R.; Ursell, T.; Wiggins, P.; Sens, P. Emerging Roles for Lipids in Shaping Membrane-Protein Function. *Nature* **2009**, *459*, 379–385.

(11) Khalifat, N.; Puff, N.; Bonneau, S.; Fournier, J. B.; Angelova, M. I. Membrane Deformation Under Local pH Gradient: Mimicking Mitochondrial Cristae Dynamics. *Biophys. J.* **2008**, *95*, 4924–4933.

(12) Hoch, F. L. Cardiolipins and Biomembrane Function. *Biochim. Biophys. Acta* **1992**, *1113*, 71–133.

(13) Daum, G. Lipids of Mitochondria. *Biochim. Biophys. Acta* **1985**, *822*, 1–42.

(14) Schlame, M.; Rua, D.; Greenberg, M. L. The Biosynthesis and Functional Role of Cardiolipin. *Prog. Lipid Res.* **2000**, *39*, 257–288.

(15) Kates, M.; Syz, J. Y.; Gosser, D.; Haines, T. H. PH-Dissociation Characteristics of Cardiolipin and its 2′-Deoxy Analogue. *Lipids* **1993**, *28*, 877–882.

(16) Haines, T. H.; Dencher, N. A. Cardiolipin: A Proton Trap for Oxidative Phosphorylation. *FEBS Lett.* **2002**, *528*, 35–39.

(17) Lewis, R. N.; McElhaney, R. N. Surface Charge Markedly Attenuates the Nonlamellar Phase-Forming Propensities of Lipid Bilayer Membranes: Calorimetric and (31)P-Nuclear Magnetic Resonance Studies of Mixtures of Cationic, Anionic, and Zwitterionic Lipids. *Biophys. J.* **2000**, *79*, 1455–1464.

(18) Marrink, S. J.; Risselada, H. J.; Yefimov, S.; Tieleman, D. P. de Vries, A. H. The MARTINI Force Field: Coarse Grained Model for Biomolecular Simulations. *J. Phys. Chem. B* **2007**, *111*, 7812–7824.

(19) Nichols-Smith, S.; Teh, S. Y.; Kuhl, T. L. Thermodynamic and Mechanical Properties of Model Mitochondrial Membranes. *Biochim. Biophys. Acta* **2004**, *1663*, 82–88.

(20) Dahlberg, M. Polymorphic Phase Behavior of Cardiolipin Derivatives Studied by Coarse-Grained Molecular Dynamics. *J. Phys. Chem. B* **2007**, *111*, 7194–7200.

(21) Seddon, J. M.; Kaye, R. D.; Marsh, D. Induction of the Lamellar-Inverted Hexagonal Phase Transition in Cardiolipin by Protons and Monovalent Cations. *Biochim. Biophys. Acta* **1983**, *734*, 347–352.

(22) Ioannou, P. V.; Golding, B. T. Cardiolipins: Their Chemistry and Biochemistry. *Prog. Lipid Res.* **1979**, *17*, 279–318.

(23) Matsumoto, K.; Kusaka, J.; Nishibori, A.; Hara, H. Lipid Domains in Bacterial Membranes. *Mol. Microbiol.* **2006**, *61*, 1110–1117.

(24) Osman, C.; Haag, M.; Potting, C.; Rodenfels, J.; Dip, P. V.; Wieland, F. T.; Brugger, B.; Westermann, B.; Langer, T. The Genetic Interactome of Prohibitins: Coordinated Control of Cardiolipin and Phosphatidylethanolamine by Conserved Regulators in Mitochondria. *J. Cell Biol.* **2009**, *184*, 583–596.

(25) Gohil, V. M.; Thompson, M. N.; Greenberg, M. L. Synthetic Lethal Interaction of the Mitochondrial Phosphatidylethanolamine and Cardiolipin Biosynthetic Pathways in Saccharomyces Cerevisiae. *J. Biol. Chem.* **2005**, *280*, 35410–35416.

(26) Gohil, V. M.; Greenberg, M. L. Mitochondrial Membrane Biogenesis: Phospholipids and Proteins Go Hand in Hand. *J. Cell Biol.* **2009**, *184*, 469–472.

(27) Helfrich, W. Elastic Properties of Lipid Bilayers: Theory and Possible Experiments. *Z. Naturforsch., C: J. Biosci.* **1973**, *28*, 693–703.

(28) Szleifer, I.; Kramer, D.; Ben-Shaul, A.; Gelbart, W. M.; Safran, S. A. Molecular Theory of Curvature Elasticity in Surfactant Films. *J. Chem. Phys.* **1990**, *92*, 6800–6817.

(29) Winterhalter, M.; Helfrich, W. Effect of Surface Charge on the Curvature Elasticity of Membranes. *J. Phys. Chem.* **1988**, *92*, 6865–6867.

(30) Andelman, D. Electrostatic Properties of Membranes: The Poisson—Boltzmann Theory. In *Handbook of Biological Physics*; Lipowsky, R., Sackmann, E., Eds.; Elsevier Science: Amsterdam, The Netherlands, 1995; pp 603.

(31) Fogden, A.; Ninham, B. W. Electrostatics of Curved Fluid Membranes: The Interplay of Direct Interactions and Fluctuations in Charged Lamellar Phases. *Adv. Colloid Interface Sci.* **1999**, *83*, 85–110.

(32) Fuller, N.; Benatti, C. R.; Rand, R. P. Curvature and Bending Constants for Phosphatidylserine-Containing Membranes. *Biophys. J.* **2003**, *85*, 1667–1674.

(33) Rowat, A. C.; Hansen, P. L.; Ipsen, J. H. Experimental Evidence of the Electrostatic Contribution to Membrane Bending Rigidity. *Europhys. Lett.* **2004**, *67*, 144–149.

(34) Dahlberg, M.; Maliniak, A. Molecular Dynamics Simulations of Cardiolipin Bilayers. *J. Phys. Chem. B.* **2008**, *112*, 11655–11663.

(35) Rog, T.; Martinez-Seara, H.; Munck, N.; Oresic, M.; Karttunen, M.; Vattulainen, I. Role of Cardiolipins in the Inner Mitochondrial Membrane: Insight Gained through Atom-Scale Simulations. *J. Phys. Chem. B* **2009**, *113*, 3413–3422.

(36) Pöyry, S.; Róg, T.; Karttunen, M.; Vattulainen, I. Mitochondrial Membranes with Mono- and Divalent Salt: Changes Induced by Salt Ions on Structure and Dynamics. *J. Phys. Chem. B* **2009**, *113*, 15513–15521.

(37) Dickey, A.; Faller, R. Examining the Contributions of Lipid Shape and Headgroup Charge on Bilayer Behavior. *Biophys. J.* **2008**, *95*, 2636–2646.

(38) Bennun, S. V.; Hoopes, M. I.; Xing, C.; Faller, R. Coarse-Grained Modeling of Lipids. *Chem. Phys. Lipids* **2009**, *159*, 59–66.

(39) Dahlberg, M.; Marini, A.; Mennucci, B.; Maliniak, A. Quantum Chemical Modeling of the Cardiolipin Headgroup. *J. Phys. Chem. A* **2010**, *114*, 4375–4387.

(40) Hess, B.; Kutzner, C.; van der Spoel, D.; Lindahl, E. GROMACS 4: Algorithms for Highly Efficient, Load-Balanced, and Scalable Molecular Simulation. *J. Chem. Theory Comp.* **2008**, *4*, 435–447.

(41) Lindahl, E.; Edholm, O. Spatial and Energetic-Entropic Decomposition of Surface Tension in Lipid Bilayers from Molecular Dynamics Simulations. *J. Chem. Phys.* **2000**, *113*, 3882–3893.

(42) Jendrasiak, G. L.; Hasty, J. H. The Hydration of Phospholipids. *Biochim. Biophys. Acta* **1974**, *337*, 79–91.

(43) Tolpekina, T. V.; den Otter, W. K.; Briels, W. J. Simulations of Stable Pores in Membranes: System Size Dependence and Line Tension. *J. Chem. Phys.* **2004**, *121*, 8014–8020.

(44) Rand, R. P.; Parsegian, V. A. Hydration Forces between Phospholipid Bilayers. *Biochim. Biophys. Acta* **1989**, *988*, 351–376.

(45) Marrink, S. J.; deVries, A. H.; Mark, A. E. Coarse Grained Model for Semiquantitative Lipid Simulations. *J. Phys. Chem. B* **2004**, *108*, 750–760.

(46) Kucerka, N.; Gallova, J.; Uhrikova, D.; Balgavy, P.; Bulacu, M.; Marrink, S. J.; Katsaras, J. Areas of Monounsaturated Diacylphosphatidylcholines. *Biophys. J.* **2009**, *97*, 1926–1932.

(47) Goormaghtigh, E.; Chatelain, P.; Caspers, J.; Ruysschaert, J. M. Evidence of a Complex between Adriamycin Derivatives and Cardiolipin: Possible Role in Cardiotoxicity. *Biochem. Pharmacol.* **1980**, *29*, 3003–3010.

(48) Goormaghtigh, E.; Huart, P.; Praet, M.; Brasseur, R.; Ruysschaert, J.-. Structure of the Adriamycin-Cardiolipin Complex: Role in Mitochondrial Toxicity. *Biophys. Chem.* **1990**, *35*, 247–257.

(49) Lewis, R. N.; Zweytick, D.; Pabst, G.; Lohner, K.; McElhaney, R. N. Calorimetric, X-Ray Diffraction and Spectroscopic Studies of the Thermotropic Phase Behavior and Organization of Tetramyristoyl Cardiolipin Membranes. *Biophys. J.* **2007**, *92*, 3166–77.

(50) Pinheiro, T. J. T.; Duralski, A. A.; Watts, A. Phospholipid Headgroup-Headgroup Electrostatic Interactions in Mixed Bilayers of Cardiolipin with Phosphatidylcholines Studied by H-2 NMR. *Biochemistry* **1994**, *33*, 4896–4902.

(51) Olbrich, K.; Rawicz, W.; Needham, D.; Evans, E. Water Permeability and Mechanical Strength of Polyunsaturated Lipid Bilayers. *Biophys. J.* **2000**, *79*, 321–327.

(52) Rawicz, W.; Olbrich, K. C.; McIntosh, T.; Needham, D.; Evans, E. Effect of Chain Length and Unsaturation on Elasticity of Lipid Bilayers. *Biophys. J.* **2000**, *79*, 328–339.

(53) Shoemaker, S. D.; Vanderlick, T. K. Intramembrane Electrostatic Interactions Destabilize Lipid Vesicles. *Biophys. J.* **2002**, *83*, 2007–2014.

(54) Baoukina, S.; Monticelli, L.; Amrein, M.; Tieleman, D. P. The Molecular Mechanism of Monolayer-Bilayer Transformations of Lung Surfactant from Molecular Dynamics Simulations. *Biophys. J.* **2007**, *93*, 3775–3782.

(55) Lindahl, E.; Edholm, O. Mesoscopic Undulations and Thickness Fluctuations in Lipid Bilayers from Molecular Dynamics Simulations. *Biophys. J.* **2000**, *79*, 426–433.

(56) Harmandaris, V. A.; Deserno, M. A Novel Method for Measuring the Bending Rigidity of Model Lipid Membranes by Simulating Tethers. *J. Chem. Phys.* **2006**, *125*, 204905.

(57) Chen, Z.; Rand, R. P. The Influence of Cholesterol on Phospholipid Membrane Curvature and Bending Elasticity. *Biophys. J.* **1997**, *73*, 267–276.

(58) Evans, E.; Heinrich, V. Dynamic Strength of Fluid Membranes. *C. R. Phys.* **2003**, *4*, 265–274.

(59) Wang, H.; de Joannis, J.; Jiang, Y.; Gaulding, J. C.; Albrecht, B.; Yin, F.; Khanna, K.; Kindt, J. T. Bilayer Edge and Curvature Effects on Partitioning of Lipids by Tail Length: Atomistic Simulations. *Biophys. J.* **2008**, *95*, 2647–2657.

(60) Karatekin, E.; Sandre, O.; Guitouni, H.; Borghi, N.; Puech, P. H.; Brochard-Wyart, F. Cascades of Transient Pores in Giant Vesicles: Line Tension and Transport. *Biophys. J.* **2003**, *84*, 1734–1749.

(61) Genco, I.; Gliozzi, A.; Relini, A.; Robello, M.; Scalas, E. Electroporation in Symmetric and Asymmetric Membranes. *Biochim. Biophys. Acta* **1993**, *1149*, 10–18.

(62) Diederich, A.; Bähr, G.; Winterhalter, M. Influence of Surface Charges on the Rupture of Black Lipid Membranes. *Phys. Rev. E* **1998**, *58*, 4883.

(63) Wohlert, J.; den Otter, W. K.; Edholm, O.; Briels, W. J. Free Energy of a Trans-Membrane Pore Calculated from Atomistic Molecular Dynamics Simulations. *J. Chem. Phys.* **2006**, *124*, 154905.

(64) Pandit, S. A.; Bostick, D.; Berkowitz, M. L. Mixed Bilayer Containing Dipalmitoylphosphatidylcholine and Dipalmitoylphosphatidylserine: Lipid Complexation, Ion Binding, and Electrostatics. *Biophys. J.* **2003**, *85*, 3120–3131.

(65) Vacha, R.; Siu, S. W.; Petrov, M.; Bockmann, R. A.; Barucha-Kraszewska, J.; Jurkiewicz, P.; Hof, M.; Berkowitz, M. L.; Jungwirth, P. Effects of Alkali Cations and Halide Anions on the DOPC Lipid Membrane. *J. Phys. Chem. A* **2009**, *113*, 7235–7243.

(66) Evans, E.; Rawicz, W. Entropy-Driven Tension and Bending Elasticity in Condensed-Fluid Membranes. *Phys. Rev. Lett.* **1990**, *64*, 2094–2097.

(67) Sennato, S.; Bordi, F.; Cametti, C.; Coluzza, C.; Desideri, A.; Rufini, S. Evidence of Domain Formation in Cardiolipin-Glycerophospholipid Mixed Monolayers. A Thermodynamic and AFM Study. *J. Phys. Chem. B* **2005**, *109*, 15950–15957.

(68) Domenech, O.; Redondo, L.; Picas, L.; Morros, A.; Montero, M. T.; Hernandez-Borrell, J. Atomic Force Microscopy Characterization of Supported Planar Bilayers that Mimic the Mitochondrial Inner Membrane. *J. Mol. Recognit.* **2007**, *20*, 546–553.

(69) Domenech, O.; Morros, A.; Cabanas, M. E.; Montero, M. T.; Hernandez-Borrell, J. Thermal Response of Domains in Cardiolipin Content Bilayers. *Ultramicroscopy* **2007**, *107*, 943–947.

(70) Sammalkorpi, M.; Karttunen, M.; Haataja, M. Micelle Fission through Surface Instability and Formation of an Interdigitating Stalk. *J. Am. Chem. Soc.* **2008**, *130*, 17977–17980.

(71) Izvekov, S.; Swanson, J. M. J.; Voth, G. A. Coarse-Graining in Interaction Space: A Systematic Approach for Replacing Long-Range Electrostatics with Short-Range Potentials. *J. Phys. Chem. B* **2008**, *112*, 4711–4724.

(72) Shi, Q.; Liu, P.; Voth, G. A. Coarse-Graining in Interaction Space: An Analytical Approximation for the Effective Short-Ranged Electrostatics. *J. Phys. Chem. B* **2008**, *112*, 16230–16237.

CT900654E